Analytic Simulation of Strongly Non-Gaussian Non-Stationary Stochastic Processes via Stochastic Adaptive Sparse Representation Based on the Iterative Method

Ying Zhang[a,1], Wei Qu[b,2] and Tao Qian[c,*]

[a]Dept of Mathematics, Zhejiang University of Science and Technology, Hangzhou 310023, China
[b]College of Sciences, China Jiliang University, Hangzhou 310018, China
[c]Macau Center for Mathematical Sciences, Macau University of Science and Technology, Macau 999078, China

ARTICLE INFO

Keywords:
Stochastic Adaptive Fourier Sparse Decomposition
Non-Gaussian stochastic process
Non-Stationary
Karhunen-Loève Expansion
Iterative Translation Approximation Method
Analytic Expansion

ABSTRACT

This paper proposes a novel method based on Stochastic Adaptive Fourier Decomposition (SAFD) for simulating non-Gaussian and non-stationary random processes with prescribed autocorrelation function (ACF) and cumulative distribution function (CDF). The method first iteratively approximates the underlying Gaussian autocorrelation matrix in the translation process, then analytically expands the target process using adaptive orthogonal basis functions. In contrast to the Karhunen-Loève (KL) expansion that requires computing eigenpairs of the autocorrelation function, SAFD directly provides an explicit analytical representation of non-Gaussian processes. Numerical experiments demonstrate that SAFD reduces approximation errors by 70-85% compared to KL at low-order expansions (e.g., 2 or 5 terms). These results show that SAFD achieves target covariance approximation with fewer expansion terms and significantly faster convergence.

1. Introduction

Uncertainty modeling, quantification, and propagation are essential in engineering design, particularly for complex systems where performance is highly sensitive to input variability [1]. Monte Carlo Simulation (MCS) is widely adopted to address uncertainties in material properties and excitation inputs [2, 3]. A key challenge lies in generating stochastic excitation samples that accurately reproduce prescribed marginal distributions, correlation structures, and higher-order statistics. Traditional methods often compromise between efficiency and accuracy. In this context, non-Gaussian random models offer enhanced flexibility and modeling capability. Furthermore, analytical formulations of stochastic processes are critical for reducing computational complexity while maintaining accuracy in practical applications. Over the past few decades, various methods have been developed to simulate non-Gaussian random processes that satisfy both a given autocorrelation function (ACF) or power spectral density function (PSDF) and marginal non-Gaussian cumulative distribution function (CDF). This is known as the "two-match problem." Existing methods can be classified into two categories: one involves checking the compatibility between the ACF (or PSDF) and the CDF [4], and using iterative algorithms to achieve approximate compatibility if necessary this is referred to as the "compatibility-constrained two-match method"; the other does not require compatibility and is called the "compatibility-free two-match method.

The compatibility-constrained two-match methods primarily rely on spectral representation for simulating non-Gaussian random processes. These methods integrate spectral representation theory with nonlinear mapping in the frequency domain. In an early contribution, Yamazaki and Shinozuka [5] proposed an iterative algorithm to identify the PSDF of the underlying Gaussian process. Subsequently, Popescu et al. [6] enhanced this framework and extended it to simulate both non-Gaussian processes and random fields. In the early 2000s, Deodatis et al. [7, 8] incorporated nonlinear mapping into the iterative scheme to better capture strong skewness in target distributions. Further improvements involved optimization techniques to eliminate undesired correlations in the iterative update. To address the high computational cost and limited accuracy of earlier methods, Lagaros et al. [9] introduced neural network-based regression models to replace the traditional PSDF update in Deodatis's algorithm. While effective, these

*Corresponding author
cnuzhangying@163.com (Y. Zhang); quwei2math@qq.com (W. Qu); tqian@must.edu.mo (T. Qian)
ORCID(s): 0000-0002-4081-9163 (Y. Zhang)

Preprint not peer reviewed
This preprint research paper has not been peer reviewed. Electronic copy available at: https://ssrn.com/abstract=5360033

methods typically require the generation of sample realizations, which significantly increase computational burden. To mitigate this, Shields et al. [10, 11] developed an efficient iterative algorithm that avoids sample generation, enabling direct estimation of the underlying Gaussian PSDF. Their work was later extended to vector-valued processes. More recent developments include spectral representation schemes that account for wave propagation effects [12], iterative transformation approximation models [13, 14], and eigenvalue-based formulations capable of handling complex-valued spectral matrices with proven convergence [15]. Additionally, EPSD-based models integrated with SRM have recently been developed to simulate nonstationary strong winds, offering a practical extension of spectral representation techniques to real-world time-varying excitations [16].

In contrast, compatibility-free two-match methods bypass the need to enforce compatibility between correlation structure and marginal distributions. The most representative approaches in this category are the Karhunen–Loève (KL) decomposition and generalized Polynomial Chaos (gPC) expansion. KL-based methods for non-Gaussian process simulation were introduced nearly two decades ago, with Phoon et al. [17, 18] being among the earliest contributors. These methods construct KL expansions in terms of non-Gaussian random variables adjusted to match prescribed marginal distributions. While effective for univariate and weakly correlated fields, KL-based simulation of non-Gaussian processes is hindered by the computational complexity of solving the second kind Fredholm integral equations. Solving such equations is highly complex and, in most cases, only numerical solutions can be obtained, making analytical expressions difficult to derive. More recently, KL-based methods have been combined with multi-fidelity iterative algorithms [19, 20] and L-moment-based Hermite polynomial expansions [21–23], with numerical schemes such as the Nyström method used to approximate eigenvalues and eigenfunctions. Despite notable improvements in dimensionality reduction and statistical accuracy, analytical expressions and convergence guarantees remain lacking. Another widely used approach is the gPC expansion, which employs multidimensional Hermite polynomials to represent non-Gaussian random processes as functions of standard Gaussian variables. This formulation allows the non-Gaussian characteristics of the target field to be modeled through the transformation of underlying Gaussian processes. In 2019, Dai et al. [24] proposed an enhanced method that integrates the KL decomposition with the gPC framework to construct explicit expressions for non-Gaussian processes. In their approach, the traditional Latin Hypercube orthogonalization technique was replaced by Hermite polynomial-based orthogonalization, which notably improved the accuracy in capturing tail behaviors and higher-order statistics of the KL random variables.However, traditional gPC methods employ fixed basis functions that do not adapt to the characteristics of the target random process, thereby limiting their flexibility and modeling adaptability. To overcome this limitation, the Adaptive Fourier Decomposition Chaos (AFD Chaos) method, based on Adaptive Fourier Decomposition, was proposed in [25] as an enhancement to conventional gPC approaches.

Overall, regardless of whether compatibility constraints are required, both categories of methods remain active areas of parallel research and have achieved significant progress in the modeling of non-Gaussian random fields and processes. In [26], we previously simulated non-Gaussian processes using the Stochastic Orthogonal Adaptive Fourier Decomposition (SPOAFD) method in conjunction with the iterative update strategy proposed by Zheng [27]. However, this approach requires the step-by-step generation of corresponding sample points to achieve the simulation, which significantly increases the computational complexity of the algorithm.

In this paper, we integrate the Iterative Transformation Approximation Method (ITAM) proposed by Shields et al. [28] with the Stochastic Adaptive Fourier Decomposition (SAFD) algorithm. By directly updating the underlying Gaussian ACF, the proposed approach improves both the accuracy and efficiency of the simulation while ensuring that the generated process satisfies both the target ACF and the prescribed non-Gaussian CDF. In the physical domain (e.g., time or frequency domain), the SAFD method can serve as an alternative to the KL decomposition or spectral representation. In the probabilistic domain, it can act as a substitute for gPC expansions. Compared with KL decomposition, the SAFD method does not require computing the eigenvalues and eigenfunctions of the kernel operator defined by the target autocorrelation function, which are typically obtainable only through numerical methods. Moreover, SAFD provides an adaptive analytical representation of the random process. Compared with spectral representation, SAFD offers greater flexibility by adaptively selecting dictionary elements as the basis functions. Moreover, relative to gPC methods, SAFD exhibits clear advantages in terms of adaptability, analytical representation capability, and modeling efficiency.

The structure of the paper is organized as follows. Section 2 introduces the proposed SAFD method. Sections 3 and 4 provide brief reviews of the Extended Translation Process Theory and the Karhunen–Loève expansion, respectively. In Section 5, the SAFD method is integrated with the ITAM approach to simulate non-Gaussian stochastic processes.

This preprint research paper has not been peer reviewed. Electronic copy available at: https://ssrn.com/abstract=5360033

Section 6 presents four numerical examples and compares the proposed method with the KL method, demonstrating its effectiveness and high accuracy. Finally, Section 7 concludes the study.

2. Stochastic Adaptive Fourier Decompositon (SAFD)

Given a probability space $(\Omega, \mathcal{F}, \mathbb{P})$, we consider a real-valued second-order stochastic process $\{f(t,\omega) : (t,\omega) \in \mathcal{T}\times\Omega\}$, where $\mathcal{T}$ denotes either the time domain or a spatial domain. The process is assumed to belong to the following Bochner space.

Definition 1. *The Bochner space $L^2(\mathcal{T},\Omega)$ [29, 30] is defined to be the Hilbert space consisting of all $L^2(\mathcal{T})$-valued random variables $f : \mathcal{T}\times\Omega \to \mathbb{R}$ satisfying*

$$\|f\|^2_{L^2(\mathcal{T},\Omega)} := \int_\Omega \int_{\mathcal{T}} |f(t,\omega)|^2 \, dt d\mathbb{P}(\omega) < \infty. \tag{1}$$

The Bochner space $L^2(\mathcal{T},\Omega)$ is a Hilbert space with the inner product defined through Bochner integral [31, 32].

This paper adopts the parameter set $\mathbf{B}_1$, which denotes the open unit disc in the complex plane, with $\partial\mathbf{B}_1$ representing its boundary. We take $\mathcal{T} = \partial\mathbf{B}_1 = \{e^{it} \mid t \in [0, 2\pi)\}$. For brevity, we denote $\mathcal{N} = L^2(\partial\mathbf{B}_1, \Omega)$. We also denote $f_\omega(e^{it}) = f(e^{it},\omega)$. Since for almost sure $\omega \in \Omega$, the function $f_\omega \in L^2(T)$, i.e., it has finite energy almost surely, it admits the following trigonometric expansion:

$$f(e^{it},\omega) = \sum_{k=-\infty}^{\infty} c_k(\omega) e^{ikt}, \quad \text{where} \quad c_k(\omega) = \frac{1}{2\pi}\int_0^{2\pi} f(e^{is},\omega)e^{-iks} ds. \tag{2}$$

The function f_ω has the direct sum decomposition $f_\omega = f^+_\omega + f^-_\omega$, where f^+_ω and f^-_ω are the non-tangential boundary values on the unit circle of the analytic functions individually, such that

$$f(e^{it},\omega) = f^+(e^{it},\omega) + f^-(e^{it},\omega) = \sum_{k=0}^{\infty} c_k(\omega)e^{ikt} + \sum_{k=-\infty}^{-1} c_k(\omega)e^{ikt} \tag{3}$$

Since f_ω is assumed to be of real-valued, we have $c_{-k}(\omega) = \overline{c_k(\omega)}$, that implies

$$f(e^{it},\omega) = 2Re\{f^+(e^{it},\omega)\} - c_0(\omega), \tag{4}$$

Due to the above relation, the analysis of a real-valued second-order stochastic process $f_\omega(e^{it})$ can be reduced to the analysis of the associated analytic random process $f^+_\omega(e^{it})$. Since $f^+_\omega(e^{it})$ is the boundary limit of the analytic function $f^+_\omega(z)$ in $\mathbf{B}_1$, complex analytic methods are available for $f_\omega(e^{it})$. The totality of such analytic functions $f^+_\omega(z)$ in the disc is identical with the stochastic Hardy space space

$$H^2_\omega(\mathbf{B}_1) = \left\{ f^+_\omega : \mathbf{B}_1\times\Omega \to \mathbb{C} \;\middle|\; \begin{array}{l} f^+(z,\omega) \text{ is a.s. analytic in } z \text{ and} \\ f^+(z,\omega) = \sum_{k=0}^{\infty} c_k(\omega) z^k, \ \|f^+_\omega\|^2_{\mathcal{N}} = \sum_{k=0}^{\infty} \mathbb{E}_\omega|c_k(\omega)|^2 < \infty \end{array} \right\} \tag{5}$$

In the following, we introduce the SAFD theory, which is developed for the expansion of functions of the f^+_ω type. If one wishes to apply SAFD to the expansion of real-valued second-order stochastic processes, this can be achieved directly via Equation (4). Therefore, we begin by introducing the function space to which f^+_ω belongs, as well as how SAFD is used to expand f^+_ω.

We are based on a dictionary $\mathcal{D}(\mathbf{B}_1)$ of the stochastic Hardy space $H^2_\omega(\mathbf{B}_1)$. By definition, a dictionary of $H^2_\omega(\mathbf{B}_1)$ consists of a class of unimodular elements whose linear span is dense in $H^2_\omega(\mathbf{B}_1)$. We work with the Szegö kernel (or the reproducing kernel) dictionary

$$\mathcal{D}(\mathbf{B}_1) \triangleq \{k_a(z)\}_{a\in\mathbf{B}_1} \triangleq \{\frac{1}{1-\overline{a}z}\}_{a\in\mathbf{B}_1}.$$

Preprint not peer reviewed

This preprint research paper has not been peer reviewed. Electronic copy available at: https://ssrn.com/abstract=5360033

We recall that the dictionary satisfies the *stochastic boundary vanishing condition* (SBVC) [33] if any but fixed function $f^+(z,\omega) \in H^2_\omega(\mathbf{B}_1)$ there holds

$$\lim_{|a|\to\partial\mathbf{B_1}} \mathbb{E}_\omega |\langle f^+_\omega, B^a_k\rangle_{L^2(\partial\mathbf{B_1})}|^2 = 0, \tag{6}$$

where $\langle\cdot\rangle_{L^2(\partial\mathbf{B_1})}$ denotes the inner product, and $\{B^a_k\}$ is the k-Takenaka-Malmquist (TM) system with the parameter $a \in \mathbf{B}_1$ to be optimally determined by the following proposition.

$$B^a_k(z) = e_a(z)\prod_{l=1}^{k-1}\frac{z-a_l}{1-\overline{a}_l z} \tag{7}$$

where $e_a = k_a/\|k_a\|$, $\|k_a\| = 1/\sqrt{1-|a|^2}$ is the normalized Szegö kernel. The kernel are generated from performing the *stochastic* maximal selection principle (SMSP) [29].

Proposition 1. *[29]Let $f^+_\omega \in H^2_\omega(\mathbf{B}_1)$, there exists $a_k \in \mathbf{B}_1$ such that*

$$a_k = \arg\sup_{a\in\mathbf{B}_1} \mathbb{E}_\omega \left|\langle f^+(\cdot,\omega) - \mu(\cdot), B^a_k\rangle\right|^2, \tag{8}$$

The finiteness of the supremum is ensured by the Cauchy-Schwarz inequality. Here, $\mu(z) = \mathbb{E}_\omega[f^+(z,\omega)]$ represents the expectation. For each k, the quantity $\mathbb{E}_\omega|\langle f^+(\cdot,\omega) - \mu(\cdot), B^a_k\rangle|^2$ in (1) may be computed by [34]

$$\begin{aligned}
&\mathbb{E}_\omega \left|\langle f^+(\cdot,\omega) - \mu(\cdot), B^a_k\rangle\right|^2 \\
&= \int_{\partial\mathbf{D}}\int_{\partial\mathbf{D}} \mathbb{E}_\omega\left[[f^+(z,\omega)-\mu(z)][\overline{f^+(s,\omega)-\mu(s)}]\right]\overline{B^a_k}(z)B^a_k(s)dzds \\
&= \int_{\partial\mathbf{D}}\int_{\partial\mathbf{D}} \mathbf{C}(s,z)\overline{B^a_k}(z)B^a_k(s)dzds. \\
&= \int_{\partial\mathbf{D}}\int_{\partial\mathbf{D}} [R(s,z)-\mu(z)\mu(s)]\overline{B^a_k}(z)B^a_k(s)dzds
\end{aligned} \tag{9}$$

We introduce the covariance function $R(s,z) := \mathbb{E}_\omega[f^+(s,\cdot)f^+(z,\cdot)]$. Thus, the optimal parameters required for SAFD expansion are computed through the autocorrelation function (ACF) $R(s,t)$. We develop the corresponding SAFD expansion for a complex-valued stochastic process.

Theorem 1. *For any $f^+(z,\omega) \in H^2_\omega(\mathbf{B}_1)$ and the parameters $\{a_k\}_k$ selected under SMSP (8),Then, there holds, in the $\mathcal{N}$-norm sense*

$$f^+(z,\omega) = \mu(z) + \sum_{k=1}^{\infty}\langle f^+(\cdot,\omega)-\mu(\cdot), B_k\rangle B_k(z), \tag{10}$$

where $\{B_k\}_{k=1}^\infty$ is the TM-system, where $B_k = B^{a_k}_k$ with the optimally selected a_k.

In practice, we use a partial sum of the series in (10) to approximate $f^+(z,\omega)$:

$$\hat{f}^+(z,\omega) = \mu(z) + \sum_{k=1}^{n}\langle f^+(\cdot,\omega)-\mu(\cdot), B_k\rangle B_k(z). \tag{11}$$

For any $f^+(e^{it},\omega) \in H^2_\omega(\partial\mathbf{B}_1)$,

$$\hat{f}^+(e^{it},\omega) = \mu(t) + \sum_{k=1}^{n}\langle f^+(\cdot,\omega)-\mu(\cdot), B_k\rangle B_k(e^{it}). \tag{12}$$

Finally, by applying Equation (4), we obtain the SAFD expansion of a real-valued stochastic process. Under mild conditions on $f^+(t,\omega)$, the convergence rate of (12) is $O\left(n^{-\frac{1}{2}}\right)$ as proved in [29]. The power of SAFD is that

Preprint not peer reviewed

This preprint research paper has not been peer reviewed. Electronic copy available at: https://ssrn.com/abstract=5360033

the selected parameters a_k's generate an orthonormal system that uniformly suits for a.s. ω, and gives rise to, as the KL method, optimal convergence rate. Besides lifting up, SAFD also finds considerable convenience regarding computation, for it can avoid using eigenvalues and eigenfunctions, the latter being necessary for the Karhunen-Loève decomposition.

3. Karhunen-Loève expansion

The KL expansion is one of the most commonly used methods to represent stochastic processes. Consider the integral operator $\mathcal{I}$ using the covariance $\mathbf{C}(s,t)$,

$$\mathcal{I}(\varphi)(s) := \int_{\mathcal{T}} \mathbf{C}(s,t)\varphi(t)dt,\ s,t \in \mathcal{T},\ \varphi(t) \in L^2(\mathcal{T}). \tag{13}$$

The solutions of the homogeneous Fredholm integral equation of the second kind

$$\int_{\mathcal{T}} \mathbf{C}(s,t)\varphi_k(t)dt = \lambda_k\varphi_k(s),\ s \in \mathcal{T}, \tag{14}$$

give rise to eigenvalues and eigenfunctions of the integral operator $\mathcal{I}$. If the covariance function $\mathbf{C}(s,t)$ meets the conditions required by the Mercer Theorem [35] then it has the following decomposition:

$$\mathbf{C}(s,t) = \sum_{k=1}^{\infty} \lambda_k\varphi_k(s)\varphi_k(t),\ s,t \in \mathcal{T}, \tag{15}$$

where φ_k's are the orthonormal eigenfunctions in $L^2(\mathcal{T})$, and the positive λ_k's are in the descent order. We obtain the KL expansion in $\mathcal{N}$

$$f(t,\omega) = \mu(t) + \sum_{k=1}^{\infty} \sqrt{\lambda_k}\varphi_k(t)\xi_k(\omega), \tag{16}$$

where $\{\xi_k(\omega)\}_k$ are the random variables given by

$$\xi_k(\omega) = \frac{1}{\sqrt{\lambda_k}} \int_{\mathcal{T}} [f(t,\omega) - \mu(t)]\varphi_k(t)dt, \tag{17}$$

which satisfy $\mathbb{E}_\omega[\xi_k] = 0,\ \mathbb{E}_\omega[\xi_k\xi_m] = \delta_{km}$, where δ_{mn} is the Kronecker-delta function. If the process is Gaussian, then $\xi_j \sim N(0,1)$ i. i. d. In practical applications, one adopts a finite truncated series expansion

$$\hat{f}(t,\omega) = \mu(t) + \sum_{k=1}^{n} \sqrt{\lambda_k}\varphi_k(t)\xi_k(\omega). \tag{18}$$

4. Extended Translation Process Theory

Grigoriu first introduced the translation process theory for constructing non-Gaussian stochastic processes [36]. Building upon this foundation, Ferrante et al. [37] developed the Extended Translation Process Theory to accommodate non-stationary processes, allowing both the marginal distribution and the correlation structure to vary with time, as discussed below.

Let $X(t)$ be a stationary Gaussian stochastic process with zero mean and unit variance. In the framework of the extended translation process theory, which allows the marginal distribution to vary with time is denoted by $F_{NG}(\cdot,t)$, the non-stationary and non-Gaussian process $Y(t)$ can be obtained by translating a Gaussian process as follows:

$$Y(t) = F_{NG}^{-1}(F_G(X(t)),t) \tag{19}$$

This preprint research paper has not been peer reviewed. Electronic copy available at: https://ssrn.com/abstract=5360033

where $F_{NG}^{-1}(\cdot,t)$ denotes the inverse of marginal non-Gaussian CDF at time t, and $F_G(\cdot)$ is the CDF of a stationary Gaussian distribution with zero mean and unit variance. Accordingly, the ACF of the translated process $Y(t)$ is given by:

$$\begin{aligned} R_{NG}(s,t) &= \mathbb{E}_\omega[Y(s)Y(t)] \\ &= \int_{-\infty}^{\infty}\int_{-\infty}^{\infty} F_{NG}^{-1}\{F_G(x_1),s\}F_{NG}^{-1}\{F_G(x_2),t\}\cdot\phi(x_1,x_2;\rho_G(s,t))dx_1dx_2. \end{aligned} \tag{20}$$

where $\phi(\cdot,\cdot;\rho_G(s,t))$ is the joint Gaussian probability density function (PDF) given by:

$$\phi(x_1,x_2;\rho_G(s,t)) = \frac{1}{\sqrt{2\pi(1-\rho_G(s,t)^2)}}\exp\left(-\frac{x_1^2+x_2^2-2\rho_G(s,t)x_1x_2}{2(1-\rho_G(s,t)^2)}\right) \tag{21}$$

where $\rho_G(s,t)$ is the correlation coefficient between $X(s)$ and $X(t)$,

$$\rho_G(s,t) = \frac{R_G(s,t)}{\sigma_G(s,s)\sigma_G(t,t)}, \tag{22}$$

$R_G(s,t)$ is the Guaasian ACF, and $\sigma_G(t,t)$ is the standard deviation of the Guassian process.

The forward translation in Eq. (20), which transforms a known Gaussian process into a specified non-Gaussian distribution, is always achievable. In contrast, the inverse transformation—where the non-Gaussian ACF is known but the Gaussian ACF is unknown—does not always yield an exact solution. In such instances, the ACF and non-Gaussian marginal distribution are considered incompatible. In non-stationary translation processes, Ferrante et al. [37] identified two types of incompatibility can arise between a given non-stationary ACF and the corresponding prescribed marginal non-Gaussian probability density function (PDF):

1. The normalized non-Gaussian correlation function $\rho_{NG}(s,t)$ can be computed similarly to Eq. (22). It has certain values that lie outside of its admissible range $[\rho_{NG}^{\min}(s,t),\rho_{NG}^{\max}(s,t)]$. The acceptable bounds for the non-Gaussian correlation distortion are calculated by setting $\rho_G(s,t)=1$ and -1 in Eq. (19) to obtain the upper and lower bounds, respectively. In the non-stationary case, the bounds on the non-Gaussian correlation are time-dependent with $\rho_{NG}^{\min}(s,t)=-\rho_{NG}^{\max}(s,t)$ if the non-Gaussian CDF is an odd function at either time s or t. Note also that the upper bound is not necessarily unity as in the stationary case. This emphasizes that in non-stationary processes, the time dependence of the normalized non-Gaussian correlation may exceed its acceptable range, leading to incompatibility.
2. The inversion of Eq. (20) results in an underlying Gaussian ACF that is not positive semi-definite (PSD). If the ACF is not PSD, it cannot be considered admissible. To check this in practice, one can compute the eigenvalues of the ACF. If any of these eigenvalues are negative, the ACF is non-PSD. The Gaussian ACF obtained through the inversion of Eq. (20) being non-PSD is equivalent to the double frequency spectral density function being non-negative. For zero-mean and unit-variance non-stationary processes, this double frequency spectral density function is defined by the following expression [37]:

$$S(u,v) = \int_{-\infty}^{\infty}\int_{-\infty}^{\infty} R(t,s)e^{i(ut-vs)}\,dtds \tag{23}$$

where u and v represent two different frequencies. If the resulting double frequency spectral density takes negative values, the ACF is incompatible.

5. Proposed ITAM with SAFD

Despite the incompatibility, the translation process model can be useful for many problems. In particular, it is valuable to identify a Gaussian process that, when translated, matches the prescribed target non-Gaussian ACF as closely as possible. This is important for problems where sensitivity to the distribution is critical, such as reliability analysis or when extreme values are of concern. For processes involving strong nonlinearities, accuracy in distribution becomes paramount. Conversely, when the response is driven primarily by correlations (e.g., in cases involving integrals over stochastic processes), it may be preferable to sacrifice some distributional accuracy in favor of a better correlation match.

Preprint not peer reviewed

This preprint research paper has not been peer reviewed. Electronic copy available at: https://ssrn.com/abstract=5360033

The proposed methodology bypasses the estimation of the double frequency spectral density function (23) by iteratively upgrading the underlying non-stationary ACF directly and simulating the process using the SAFD method. This new method, denoted SAFD-ITAM, for estimating the underlying Gaussian ACF follows these general steps:

1. Initialize the underlying Gaussian ACF. Given a prescribed pair of marginal non-Gaussian CDF and non-stationary ACF, select an arbitrary underlying Gaussian ACF as an initial guess. The ACF must satisfy all conditions of a valid ACF. Practically, this can be achieved by selecting the target non-Gaussian ACF as the initial underlying Gaussian ACF.
2. Compute the non-Gaussian ACF using non-stationary translation process theory. Specifically, calculate the non-Gaussian and non-stationary ACF from the prescribed underlying Gaussian and non-stationary ACF using translation process theory (19). To accomplish this, the normalized Gaussian correlation function is computed as:

$$\rho_G^{(i)}(s,t) = \frac{R_G^{(i)}(s,t)}{\sqrt{R_G^{(i)}(t,t) \cdot R_G^{(i)}(s,s)}} \tag{24}$$

   where $R_G^{(i)}(t,t)$ is the variance of the underlying Gaussian process at time t. The normalized Gaussian ACF is translated to the non-Gaussian ACF using Eq. (20).
3. Upgrade the underlying Gaussian ACF. If the procedure is not converged at iteration i, upgrade the underlying Gaussian ACF for iteration $i+1$ using the following equation:

$$R_G^{(i+1)}(s,t) = \frac{R_{NG}^T(s,t)}{R_{NG}^{(i)}(s,t)} R_G^{(i)}(s,t) \tag{25}$$

   This equation is based on the upgrading equation in Shields and Deodatis [11]. However, the upgraded ACF is not strictly non-negative in contrast with the evolutionary spectrum (ES) (23) in the standard ITAM. For this reason, the exponent β is eliminated, as any non-integer exponent will produce imaginary numbers when the signs of $R_G^{(i)}(s,t)$ and $R_N^T(s,t)$ differ. Furthermore, the new upgrading equation does not guarantee that the upgraded ACF is PSD. Consequently, an additional step for maintaining the PSD property of the ACF at each iteration is necessary.
4. Find the nearest positive semi-definite (PSD) ACF to the upgraded Gaussian ACF. Given an arbitrary real, symmetric Guassian ACF matrix $\mathbf{R}_G$, Higham [38] proposed a method for calculating its nearest correlation matrix in Frobenius norm by solving:

$$\begin{aligned} &\min \|\mathbf{R}_G - \hat{\mathbf{R}}\|_F \\ &\text{s.t.} \quad \hat{\mathbf{R}} = \hat{\mathbf{R}}^T,\ \mathrm{Diag}(\hat{\mathbf{R}}) = e,\ \hat{\mathbf{R}} \geq 0 \end{aligned} \tag{26}$$

   where e is the unit vector, $\hat{\mathbf{R}}$ is the nearest PSD matrix, and $\mathrm{Diag}(\hat{\mathbf{R}})$ denotes a vector of the diagonal elements of $\hat{\mathbf{R}}$. The method utilizes convex analysis to identify the solution, and it is shown to converge linearly to the solution. Subsequently, Qi and Sun presented a quadratically convergent Newton method for finding the nearest correlation matrix by dualizing Eq. (14) to an unconstrained convex optimization problem. Although various methodologies exist for computing the nearest PSD matrix, the method of Qi and Sun is utilized here due to its rapid convergence. This step is implemented after upgrading the underlying Gaussian ACF at each iteration.
5. Check the difference between the estimated and target ACFs, and iterate back to step 2 if necessary. At each iteration, the relative difference between the target non-Gaussian non-stationary ACF and the computed one is determined by:

$$\epsilon^{(i)} = 100 \times \sqrt{\frac{\sum_{n=0}^{N}\sum_{m=1}^{M}\left[R_{NG}^{(i)}(s_n,t_m) - R_{NG}^T(s_n,t_m)\right]^2}{\sum_{n=0}^{N}\sum_{m=1}^{M}\left[R_{NG}^T(s_n,t_m)\right]^2}} \tag{27}$$

   where N is the number of time intervals in the discretized domain. According to the value of the relative difference, the iterative procedure will continue or stop. Specifically, when the difference stabilizes to a constant value, the iterations are stopped.

Preprint not peer reviewed

This preprint research paper has not been peer reviewed. Electronic copy available at: https://ssrn.com/abstract=5360033

6. Simulate the process using the SAFD method. After establishing a suitable non-Gaussian ACF along with its corresponding Gaussian ACF, generating non-Gaussian sample functions with the prescribed CDF $F_{NG}(\cdot)$ becomes straightforward. Gaussian sample functions are first generated using Eq. (12) and then mapped to $F_{NG}(\cdot)$ via Eq. (19). This process does not require iterations. The resulting non-Gaussian samples reflect the non-Gaussian ACF and the given CDF in an ensemble average sense, enabling efficient simulation of multiple samples.

The iterative method produces a Gaussian ACF that closely matches the target non-Gaussian, non-stationary ACF. Once the underlying Gaussian ACF is determined, the Gaussian process is simulated using the SAFD expansion in Eq. (12), and the generated functions are mapped to the non-Gaussian form, avoiding the need to directly identify the non-Gaussian random variable distribution. The overall procedure is summarized in the flowchart shown in Fig. 1 and detailed in Algorithm 1. The effectiveness of the proposed approach is illustrated through several numerical examples in the following section.

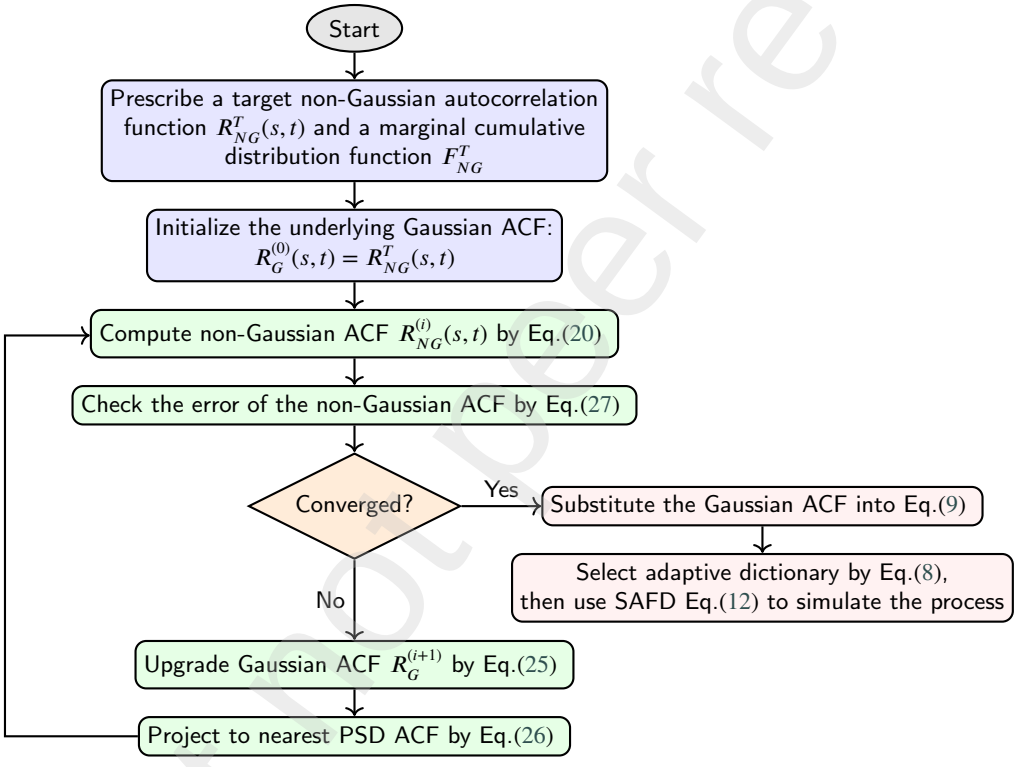


Figure 1: Flowchart of proposed SAFD-ITAM methodology.

6. Numerical examples

To assess the efficiency of the proposed methodology, a series of numerical examples are investigated, encompassing stationary and non-stationary, as well as strongly and weakly non-Gaussian stochastic processes. Furthermore, illustrative examples are provided to elucidate the two types of translation process incompatibilities discussed in Section 4. The adopted numerical examples include both the original cases and their modified counterparts as presented in Shields et al. [28].

6.1. Comparison with the SAFD-based ITAM and KL-based ITAM

We use four examples to verify the effectiveness of SAFD-ITAM, which cover both stationary and non-stationary processes, and both weakly and strongly non-Gaussian cases. The results will be compared with those of KL-ITAM. In these examples, the interval $[0, 2\pi]$ is uniformly divided into 200 parts, and the number of samples is set to 10000. It is

This preprint research paper has not been peer reviewed. Electronic copy available at: https://ssrn.com/abstract=5360033

Algorithm 1 Simulating Non-Gaussian Random Processes Based on the SAFD-ITAM Method

1: Discretize the spatial domain $\partial\mathbf{B}_1$ as $t = \{t_1, t_2, \cdots, t_M\}$, and set the initial underlying Gaussian ACF matrix as the target non-Gaussian ACF matrix: $R_G^{(0)}(t_m, t_n) = R_{NG}^T(t_m, t_n)$, for $m, n = 1, \cdots, M$.
2: Set iteration index $i \leftarrow 0$.
3: **while** the difference $\epsilon^{(i)}$ is greater than the desired threshold **do**
4: Compute the non-Gaussian ACF $R_{NG}^{(i)}(t_m, t_n)$ by

$$R_{NG}^{(i)}(t_m, t_n) = \int_{-\infty}^{\infty}\int_{-\infty}^{\infty} F_{NG}^{-1}\{F_G(x_1), t_m\} \cdot F_{NG}^{-1}\{F_G(x_2), t_n\} \cdot \phi(x_1, x_2; \rho_G^{(i)}(t_m, t_n))\, dx_1 dx_2, \tag{28}$$

where

$$\rho_G^{(i)}(t_m, t_n) = \frac{R_G^{(i)}(t_m, t_n)}{\sqrt{R_G^{(i)}(t_m, t_m) \cdot R_G^{(i)}(t_n, t_n)}} \tag{29}$$

5: Compute the difference between the estimated and target ACFs:

$$\epsilon^{(i)} = 100 \times \sqrt{\frac{\sum_{m=1}^{M}\sum_{n=1}^{M}\left[R_{NG}^{(i)}(t_m, t_n) - R_{NG}^{T}(t_m, t_n)\right]^2}{\sum_{m=1}^{M}\sum_{n=1}^{M}\left[R_{NG}^{T}(t_m, t_n)\right]^2}} \tag{30}$$

Once $\epsilon^{(i)}$ stabilizes or is below a given tolerance, terminate the iteration. Otherwise, update the Gaussian ACF.
6: Increment iteration index: $i \leftarrow i + 1$
7: Update the underlying Gaussian ACF:

$$R_G^{(i+1)}(t_m, t_n) = \frac{R_{NG}^T(t_m, t_n)}{R_{NG}^{(i)}(t_m, t_n)} \cdot R_G^{(i)}(t_m, t_n) \tag{31}$$

8: Find the nearest positive semi-definite (PSD) matrix $\hat{\mathbf{R}}$ to the updated ACF:

$$\begin{aligned} &\min \|\mathbf{R_G} - \hat{\mathbf{R}}\|_{\mathbf{F}} \\ &\text{s.t.} \quad \hat{\mathbf{R}} = \hat{\mathbf{R}}^{\top}, \quad \mathrm{Diag}(\hat{\mathbf{R}}) = \boldsymbol{e}, \quad \hat{\mathbf{R}} \succeq 0 \end{aligned} \tag{32}$$

where $\|\cdot\|_F$ denotes the Frobenius norm, $\boldsymbol{e}$ is the unit vector, and $\hat{\mathbf{R}}$ is symmetric and PSD.
9: **end while**
10: Substitute the selected semi-define $R_G^{(i+1)}$ into Eq. (9), i.e.

$$\mathbb{E}_\omega\left|\langle f_G^+(\cdot,\omega) - \mu(\cdot), B_k^a\rangle\right|^2 = \int_{\partial\mathbf{B}_1}\int_{\partial\mathbf{B}_1} [R_G^{(i+1)}(t_m, t_n) - \mu(t_m)\mu(t_n)]\overline{B_k^a}(t_m)B_k^a(t_n)dt_m dt_n \tag{33}$$

11: Use the sparse matching search principle (SMSP) to select the optimal dictionary parameter:

$$a_k = \arg\sup_{a\in D} \mathbb{E}_\omega\left|\langle f_G^+(\cdot,\omega) - \mu(\cdot), B_k^a\rangle\right|^2 \tag{34}$$

12: Simulate the underlying Gaussian process using the SAFD expansion:

$$\hat{f}_G^+(z,\omega) = \mu(z) + \sum_{k=1}^{n}\langle f_G^+(\cdot,\omega) - \mu(\cdot), B_k\rangle B_k(z) \tag{35}$$

13: Obtain a real-valued stochastic process via:

$$f_G(e^{it},\omega) = 2Re\{f_G^+(e^{it},\omega)\} - c_0(\omega) \tag{36}$$

14: Map the simulated Gaussian samples to the target non-Gaussian field:

$$f_{NG}(t) = F_{NG}^{-1}(F_G(f_G(t)), t) \tag{37}$$

well known that for a zero-mean random process, the autocorrelation function coincides with the covariance function. Therefore, without loss of generality, we assume that all random processes in the following examples are zero-mean, so that the specified covariance functions also serve as the corresponding autocorrelation functions.

Example 6.1. Stationary Weakly Non-Gaussian Process *We consider a stationary random process with a weakly non-Gaussian marginal distribution that follows a Beta distribution. The CDF is given by*

$$G(y; p, q) = \frac{\Gamma(p+q)}{\Gamma(p)\Gamma(q)}\int_0^u z^{p-1}(1-z)^{q-1}dz, \tag{38}$$

Preprint not peer reviewed

This preprint research paper has not been peer reviewed. Electronic copy available at: https://ssrn.com/abstract=5360033

where $\Gamma(\cdot)$ *denotes the Gamma function, and*

$$u = \frac{y - y_{\min}}{y_{\max} - y_{\min}}, \tag{39}$$

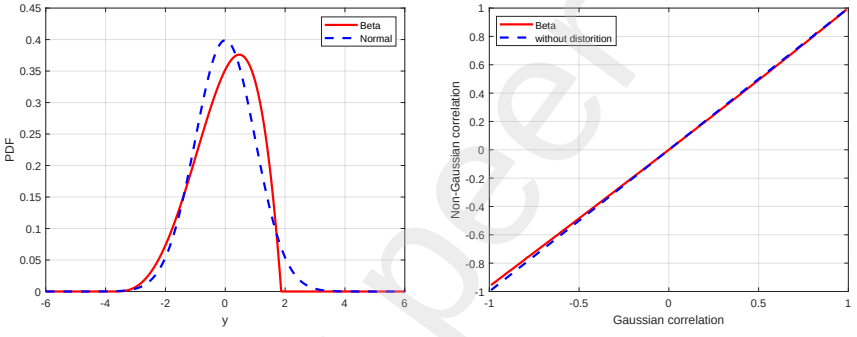
where $y_{\min} = -3.74$ *and* $y_{\max} = 1.87$ *represent the lower and upper bounds of the distribution, respectively.*

The shape parameters of the Beta distribution are set to $p = 4$ *and* $q = 2$*, such that the resulting random variable has zero mean and unit variance. As shown in Fig. 2, the distortion in the correlation structure introduced by the Beta transformation is relatively small compared to its Gaussian counterpart. Hence, the process is referred to as weakly non-Gaussian.*

The following two stationary covariance functions are considered as the target:

$$\begin{aligned} C_1(s,t) &= \exp(-|s-t|), \quad \forall s,t \in [0, 2\pi], \\ C_2(s,t) &= \exp(-|s-t|^2), \quad \forall s,t \in [0, 2\pi]. \end{aligned} \tag{40}$$

The spatial patterns and features of these covariance functions are illustrated in Fig. 3.



(a) Beta vs Gaussian (b) Correlation distortion of Beta PDF

Figure 2: Comparison of weakly non-Gaussian features: (a) beta vs Gaussian marginal PDF; (b) correlation distortion

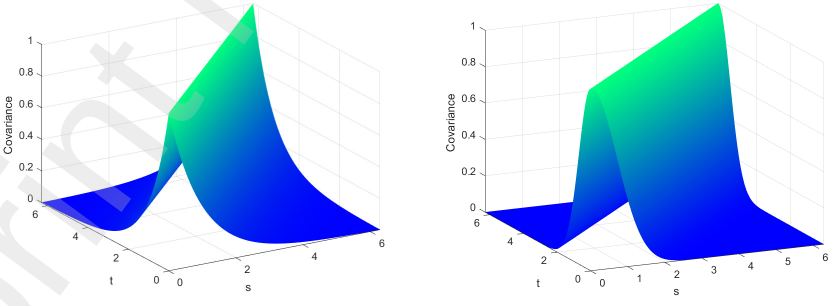


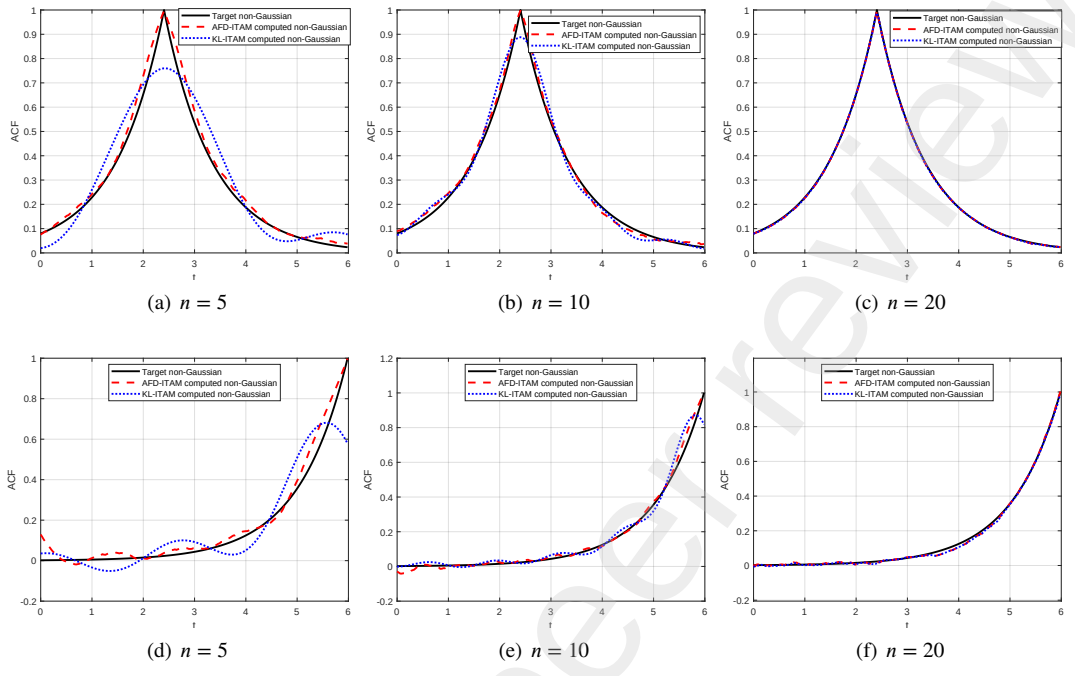
Figure 3: Target stationary covariances $\mathbf{C}_1$ and $\mathbf{C}_2$.

Figures 4 and 5 further compare the target non-Gaussian ACF with those computed by SAFD-ITAM and KL-ITAM. In Fig. 4, two representative rows of the covariance function $\mathbf{C}_1$ are selected (the 81st and 200th), with truncation terms $n = 5, 10, 20$. The black solid line represents the target non-Gaussian ACF, the red dashed line represents the SAFD-ITAM result, and the blue dotted line represents the KL-ITAM result. Although the rows are selected arbitrarily, the results clearly show that SAFD-ITAM provides better fitting performance, particularly near the peaks and boundaries,

Preprint not peer reviewed

This preprint research paper has not been peer reviewed. Electronic copy available at: https://ssrn.com/abstract=5360033

even with a small number of truncation terms. Similarly, Fig. 5 presents two arbitrarily selected rows (the 50th and 150th) from $\mathbf{C}_2$, with truncation terms $n = 5, 8, 60$, and demonstrates the same trend. These examples illustrate the fast convergence and strong approximation capability of the SAFD method.



(a) $n = 5$ (b) $n = 10$ (c) $n = 20$

(d) $n = 5$ (e) $n = 10$ (f) $n = 20$

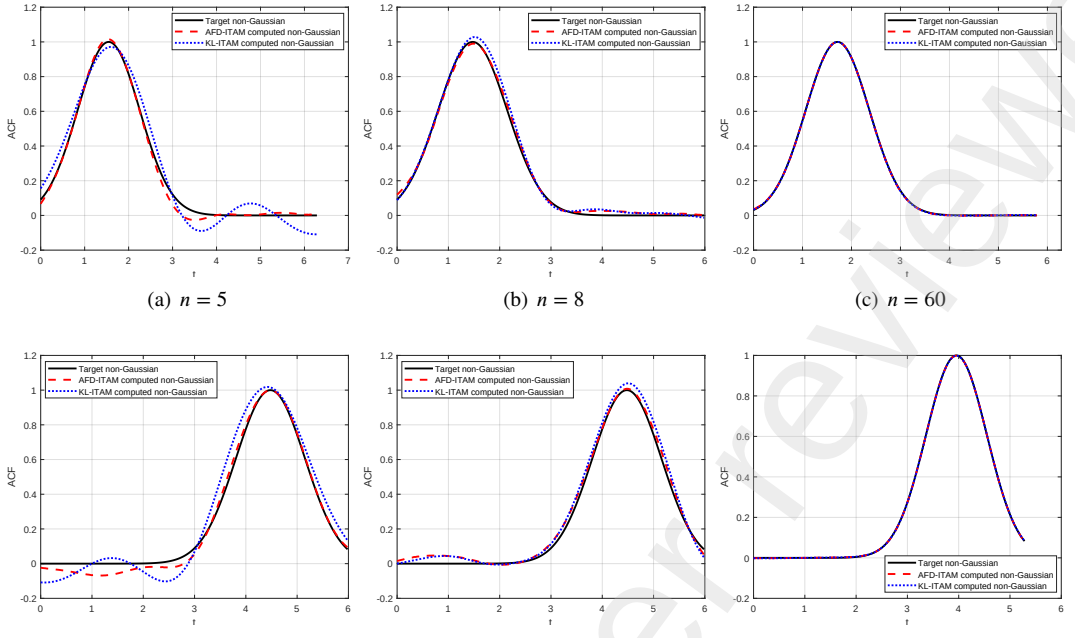
Figure 4: Comparison of target non-Gaussian, AFD-ITAM computed non-Gaussian, and KL-ITAM computed non-Gaussian ACFs. Top row: results for the $81st$ row of $\mathbf{C}_1$ with different truncation terms n; bottom row: corresponding results for the $200th$ row of $\mathbf{C}_1$.

To provide a more intuitive comparison, Figures 6 and 7 illustrate the relative error distributions and ACF reconstruction accuracy for both SAFD-ITAM and KL-ITAM when the truncation term is fixed at $n = 5$. As shown in Figure 6, SAFD-ITAM yields lower and more uniformly distributed relative errors. Figure 7 further confirms that SAFD-ITAM better preserves the non-Gaussian ACF structure, especially near key regions.

Tables 1 and 2 compare the row-wise relative errors in the covariance matrices $\mathbf{C}_1$ and $\mathbf{C}_2$ under different truncation terms, using the KL and SAFD simulation methods. Specifically, Table 1 reports errors for the 10th, 50th, 80th, and 150th rows of $\mathbf{C}_1$, while Table 2 presents results for the 5th, 15th, 40th, and 60th rows of $\mathbf{C}_2$. The results demonstrate that as the truncation term increases (e.g., from $n = 2$ to $n = 20$), both methods show a clear decline in approximation error, indicating good convergence. However, when the truncation term is small (e.g., $n = 2$ or $n = 5$), the SAFD method consistently achieves lower relative errors than the KL method across the selected rows. This highlights the superior approximation capability and faster convergence of the SAFD approach. Even as the term number increases, SAFD retains a slight performance advantage.

Preprint not peer reviewed

This preprint research paper has not been peer reviewed. Electronic copy available at: https://ssrn.com/abstract=5360033



(a) $n = 5$ (b) $n = 8$ (c) $n = 60$

(d) $n = 5$ (e) $n = 8$ (f) $n = 60$

Figure 5: Comparison of target non-Gaussian, SAFD-ITAM computed non-Gaussian, and KL-ITAM computed non-Gaussian ACFs. Top row: results for the $50th$ row of $\mathbf{C}_2$ with different truncation terms n; bottom row: corresponding results for the $150th$ row of $\mathbf{C}_2$.

Table 1
Comparison of row-wise relative errors in covariance matrice $\mathbf{C}_1$ across term.

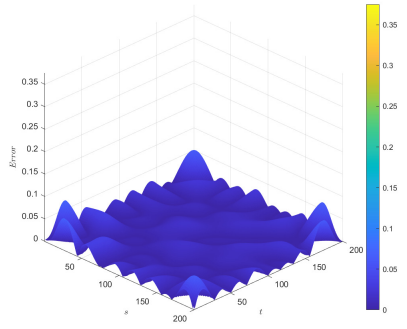
Simulated method	**KL**				**SAFD**			
term	2	5	8	20	2	5	8	20
10th row of $\mathbf{C}_1$	1.3441	0.2326	0.0154	0.0189	0.3243	0.0631	0.0270	0.0214
50th row of $\mathbf{C}_1$	0.8802	0.1646	0.0216	0.0179	0.2583	0.0278	0.0107	0.0197
80th row of $\mathbf{C}_1$	0.9596	0.1956	0.0208	0.0173	0.2652	0.0291	0.0149	0.0154
150th row of $\mathbf{C}_1$	0.8922	0.1522	0.0289	0.0188	0.2704	0.0247	0.0208	0.0177

Table 2
Comparison of row-wise relative errors in covariance matrice $\mathbf{C}_2$ across term.

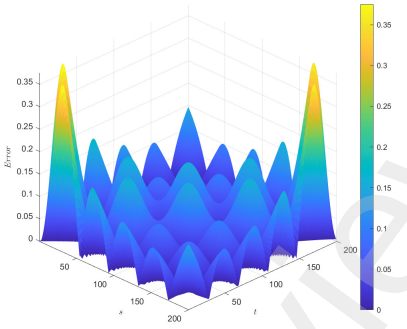
Simulated method	**KL**				**SAFD**			
term	2	5	8	20	2	5	8	20
5th row of $\mathbf{C}_2$	1.5462	0.3393	0.0381	0.0020	0.3723	0.0699	0.0358	0.0040
15th row of $\mathbf{C}_2$	1.2205	0.1580	0.0299	0.0019	0.2929	0.0491	0.0285	0.0025
40th row of $\mathbf{C}_2$	0.9097	0.2112	0.0230	0.0018	0.2555	0.0390	0.0216	0.0013
60th row of $\mathbf{C}_2$	0.9066	0.1098	0.0166	0.0019	0.2759	0.0280	0.0151	0.0029

Preprint not peer reviewed

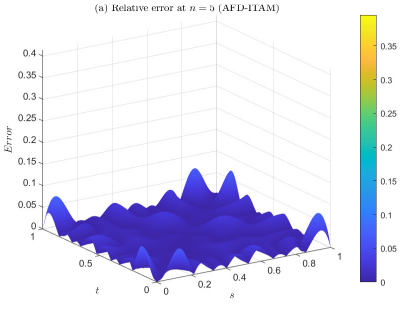
This preprint research paper has not been peer reviewed. Electronic copy available at: https://ssrn.com/abstract=5360033



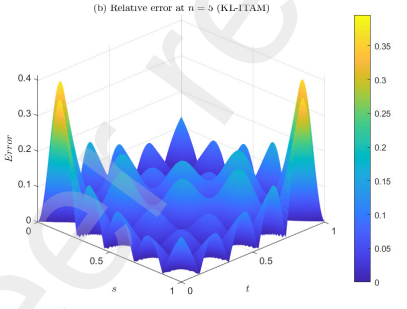
(a) relative error at $n = 5$ (SAFD-ITAM)



(b) relative error at $n = 5$ (KL-ITAM)



(c) relative error at $n = 5$ (SAFD-ITAM)



(d) relative error at $n = 5$ (KL-ITAM)

Figure 6: Comparison of relative errors between target and simulated covariances obtained via SAFD-ITAM and KL-ITAM with truncation term $n = 5$. The first row shows the results for $\mathbf{C}_1$, while the second row displays those for $\mathbf{C}_2$.

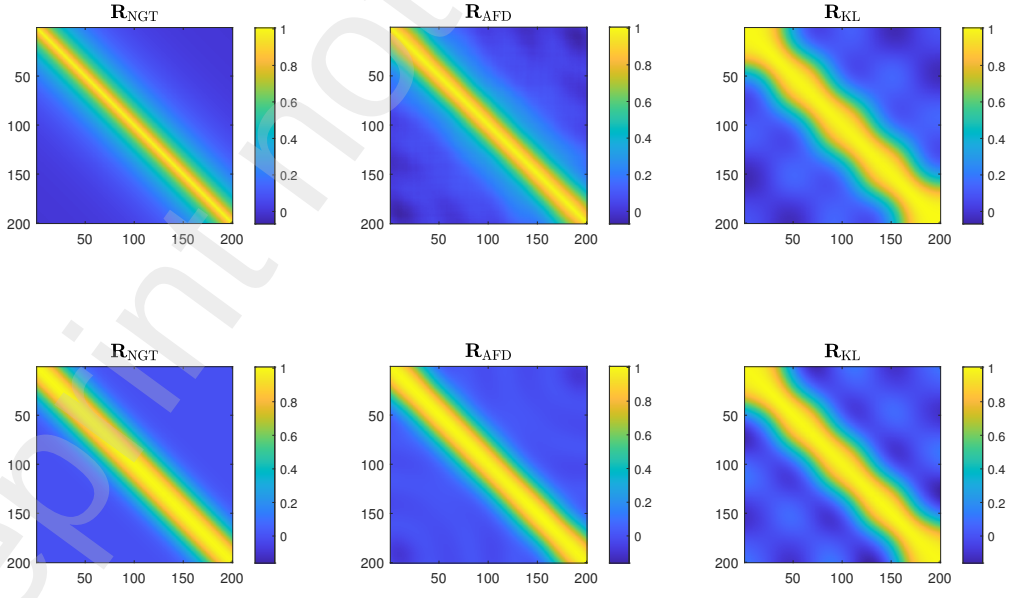


Figure 7: Comparison of non-Gaussian ACFs for different methods at truncation term $n = 5$. Top row: target, SAFD-ITAM computed, and KL-based computed ACFs for $\mathbf{C}_1$; bottom row: corresponding ACFs for $\mathbf{C}_2$.

This preprint research paper has not been peer reviewed. Electronic copy available at: https://ssrn.com/abstract=5360033

Example 6.2. Stationary strongly non-Gaussian process *The marginal non-Gaussian cumulative distribution function in this example is a shifted log-normal distribution, with the CDF defined as*

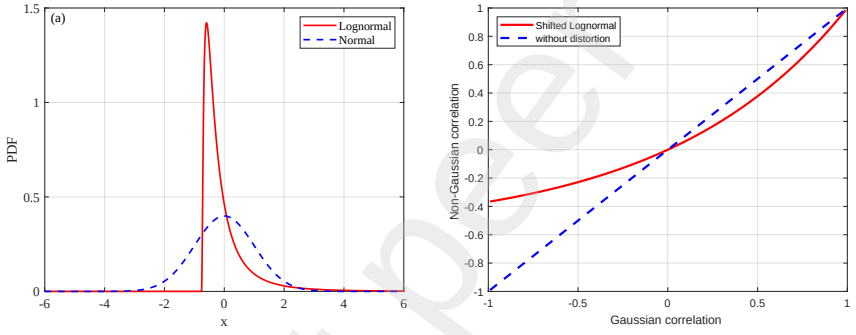
$$G(y;\mu,\sigma,\delta) = \Phi\left(\frac{\ln(y-\delta)-\mu}{\sigma}\right) \tag{41}$$

The parameters $\mu = -0.7707$, $\sigma = 1$, *and* $\delta = -0.7628$ *are selected to ensure zero mean and unit variance. As illustrated in Fig. 8 (a), this shifted log-normal distribution exhibits a strongly non-Gaussian marginal with significant deviation from the Gaussian case. Fig. 8 (b) further shows the nonlinear correlation distortion.*

The following target stationary non-Gaussian autocovariance functions are considered, as visualized in Fig. 9:

$$\begin{aligned}\mathbf{C}_3(s,t) &= \exp(-|s-t|)\cdot\cos[4\pi(s-t)]\\ \mathbf{C}_4(s,t) &= \exp(-|s-t|^2)\cdot\cos[4\pi(s-t)]\end{aligned} \tag{42}$$

These represent stationary covariance structures with oscillatory components, designed to assess the performance of the proposed non-Gaussian simulation method.



(a) Shifted lognormal vs Gaussian (b) Correlation distortion of Beta process

Figure 8: Comparison of strongly non-Gaussian features: (a) shifted lognormal vs Gaussian marginal PDF; (b) correlation distortion

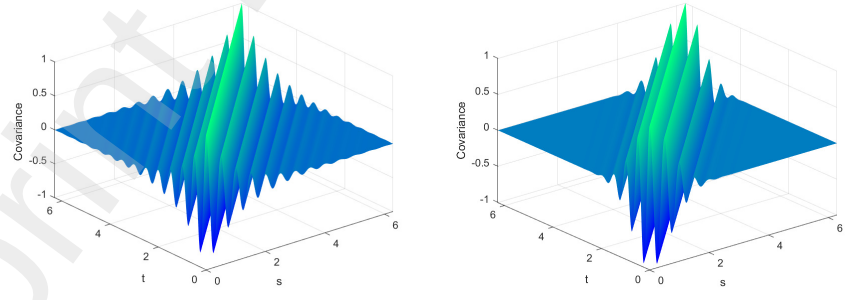


Figure 9: Target stationary covariances $\mathbf{C}_3$ and $\mathbf{C}_4$.

In the case of strongly non-Gaussian processes, Figures 10 and 11 illustrate the comparisons between the target non-Gaussian ACFs and those reconstructed by SAFD-ITAM and KL-ITAM under various truncation terms n. Specifically, the top rows of each figure show the 10th row of the target covariance matrices $\mathbf{C}_3$ and $\mathbf{C}_4$, while the bottom rows correspond to the 50th row of each matrix.

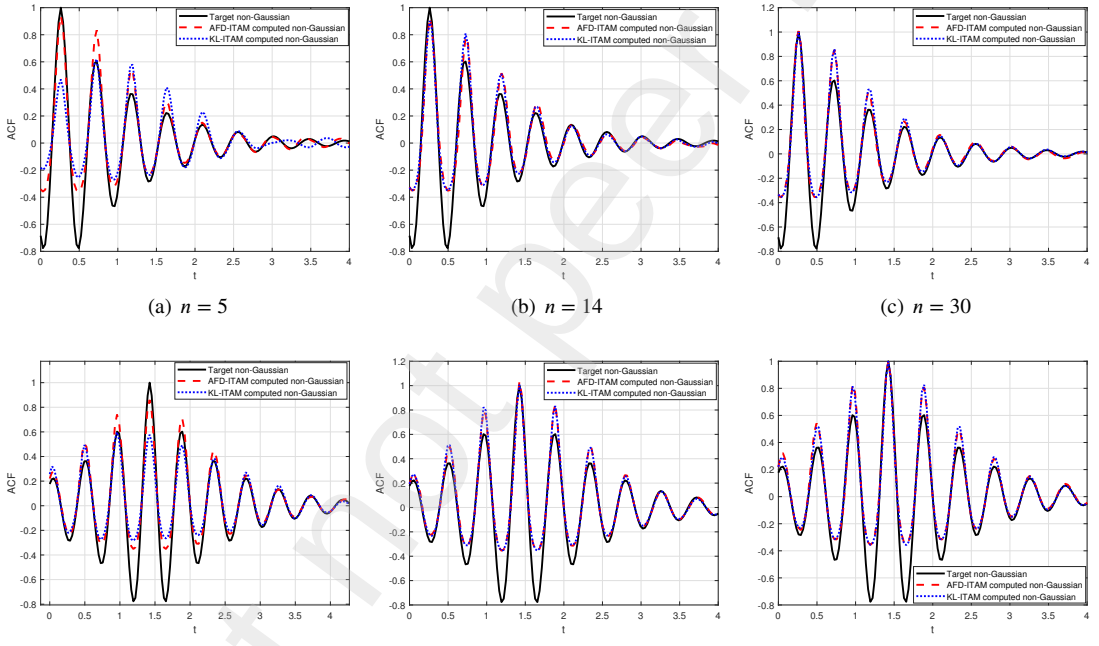
Preprint not peer reviewed

This preprint research paper has not been peer reviewed. Electronic copy available at: https://ssrn.com/abstract=5360033

As shown in Figure 10, both methods can effectively capture the oscillatory features of $\mathbf{C}_3$ under this strongly non-Gaussian condition. However, the reconstruction accuracy of both SAFD-ITAM and KL-ITAM remains limited, with relatively large approximation errors. Despite this, SAFD-ITAM demonstrates faster convergence even in cases of strong deviation from Gaussianity, and consistently produces results closer to the target when n is very small. As n increases, both methods improve in accuracy, but SAFD-ITAM still outperforms KL-ITAM in preserving the main oscillatory patterns and peak alignment of the target ACF.

Similarly, Figure 11 presents the results for $\mathbf{C}_4$. Despite its more complex structure, SAFD-ITAM provides better agreement with the target ACF across all truncation levels. In contrast, KL-ITAM tends to introduce slight distortions, especially at lower n, while SAFD-ITAM exhibits stronger robustness.

To further demonstrate the rapid convergence property of SAFD-ITAM, Figure 12 presents the spatial distribution of relative errors between the target and the simulated covariance functions when $n = 5$. The results clearly indicate that SAFD-ITAM produces significantly lower and more spatially concentrated errors, especially along the diagonal, reflecting superior local reconstruction accuracy. Figure 13 further compares the full covariance matrices $\mathbf{C}_3$ and $\mathbf{C}_4$. The SAFD-based results more accurately reconstruct the oscillatory structures of the target ACFs, whereas KL-ITAM introduces certain distortions in waveform and attenuation in oscillation strength, particularly in the high-frequency components of $\mathbf{C}_4$.



(a) $n = 5$ (b) $n = 14$ (c) $n = 30$

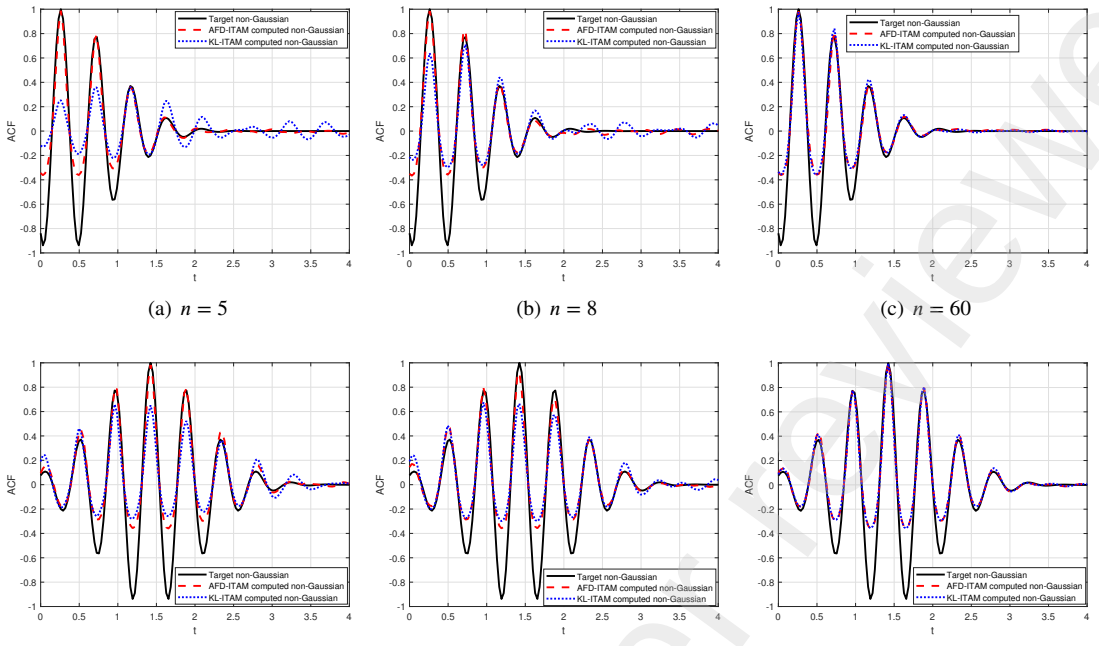
(d) $n = 5$ (e) $n = 14$ (f) $n = 30$

Figure 10: Comparison of target non-Gaussian, SAFD-ITAM computed non-Gaussian, and KL-ITAM computed non-Gaussian ACFs. Top row: results for the $10th$ row of $\mathbf{C}_3$ with different truncation terms n; bottom row: corresponding results for the $50th$ row of $\mathbf{C}_3$.

These findings further validate that the proposed SAFD-ITAM method is capable of effectively capturing complex non-Gaussian characteristics even with small truncation terms. Table 3 provides the corresponding global relative errors across different truncation levels. In all cases, the SAFD method based on SAFD-ITAM yields lower or comparable errors than the KL-based method, confirming its effectiveness in approximating strongly non-Gaussian stationary processes with oscillatory covariance structures.

Example 6.3. Non-stationary weakly non-Gaussian process *The example is also chosen as the Bata marginal distribution function in (8(a)). The target marginal distribution function changes with t. We can be rewrite (39) in*

This preprint research paper has not been peer reviewed. Electronic copy available at: https://ssrn.com/abstract=5360033



(a) $n = 5$ (b) $n = 8$ (c) $n = 60$

(d) $n = 5$ (e) $n = 8$ (f) $n = 11$

Figure 11: Comparison of target non-Gaussian, SAFD-ITAM computed non-Gaussian, and KL-ITAM computed non-Gaussian ACFs. Top row: results for the $10th$ row of $\mathbf{C}_4$ with different truncation terms n; bottom row: corresponding results for the $50th$ row of $\mathbf{C}_4$.

Table 3
Comparison of global relative errors of covariance matrices across term.

Covariance Matrix	KL				SAFD			
	5	8	12	23	5	8	12	23
$\mathbf{C}_3$	0.5053	0.4218	0.3495	0.3327	0.3681	0.3451	0.3362	0.3379
$\mathbf{C}_4$	0.4010	0.3956	0.3837	0.3735	0.3997	0.3918	0.3886	0.3710

this form

$$u(t) = \frac{y(t) - y_{min}(t)}{y_{max}(t) - y_{min}(t)} \tag{43}$$

where

$$y_{min}(t) = \mu_B(t) - \sigma_B(t)\sqrt{\frac{p(p+q+1)}{q}}, \qquad y_{max}(t) = \mu_B(t) + \sigma_B(t)\sqrt{\frac{q(p+q+1)}{p}}. \tag{44}$$

The covariance function is constructed based on the non-stationary Brown-Bridge model. As shown in Fig. 14 (a), the target non-stationary covariance function exhibits variance characteristics dependent on t. The Brown-Bridge covariance function is given by

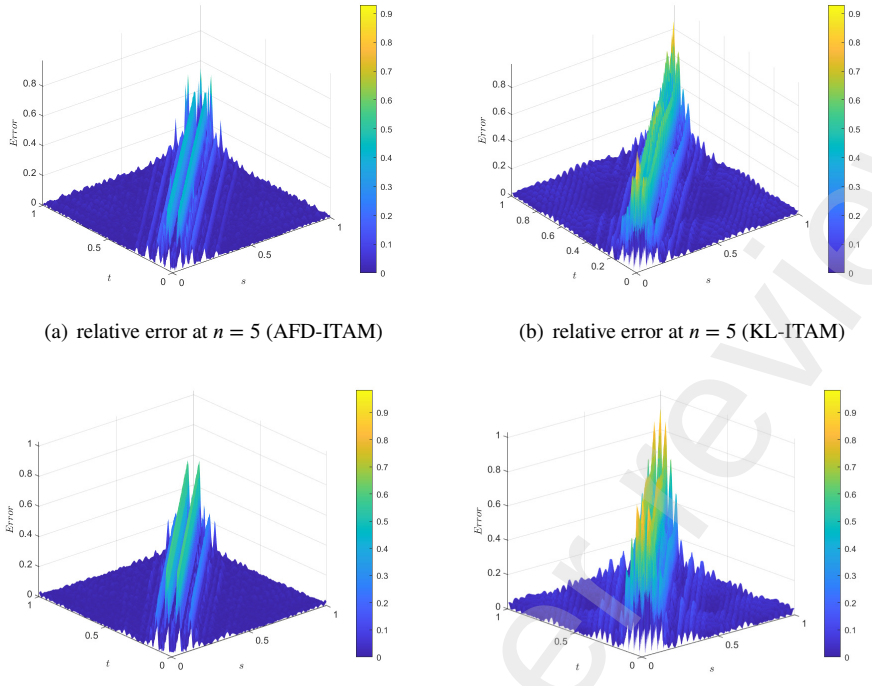
$$\mathbf{C}_5(s,t) = min(s,t) - \frac{st}{2\pi}, \quad \forall s,t \in [0, 2\pi] \tag{45}$$

and the variance is obtained to be

$$\sigma_B^2(t) = R_3(t,t) = min(t,t) - \frac{st}{2\pi} = t - \frac{t^2}{2\pi}, \quad \forall t \in [0, 2\pi] \tag{46}$$

Preprint not peer reviewed

This preprint research paper has not been peer reviewed. Electronic copy available at: https://ssrn.com/abstract=5360033



(a) relative error at $n = 5$ (AFD-ITAM)

(b) relative error at $n = 5$ (KL-ITAM)

(c) relative error at $n = 5$ (AFD-ITAM)

(d) relative error at $n = 5$ (KL-ITAM)

Figure 12: Comparison of relative errors between target and simulated covariances obtained via SAFD-ITAM and KL-ITAM with truncation term $n = 5$. The first row shows the results for $\mathbf{C}_3$, while the second row displays those for $\mathbf{C}_4$.

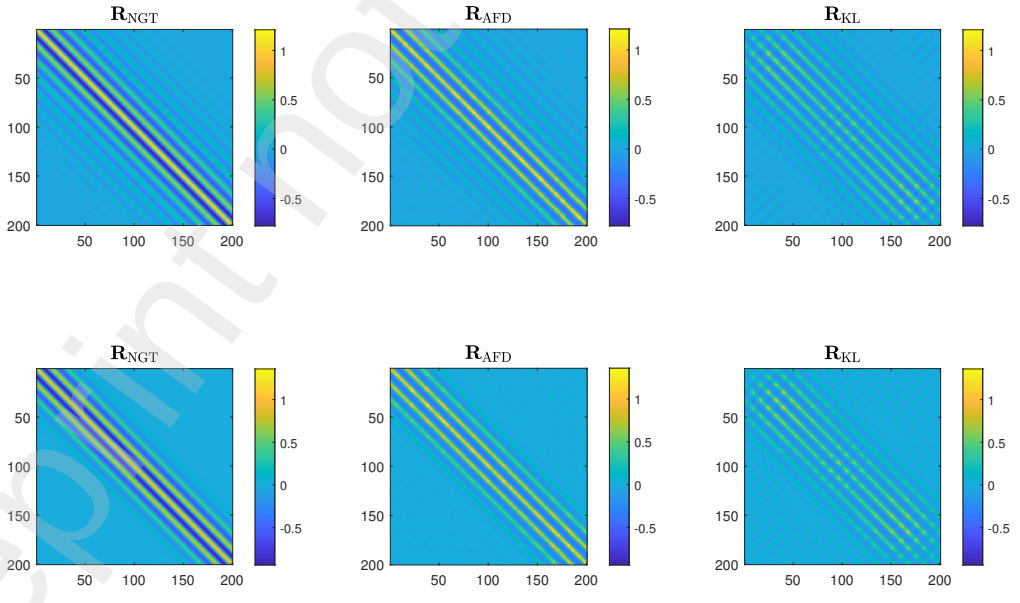


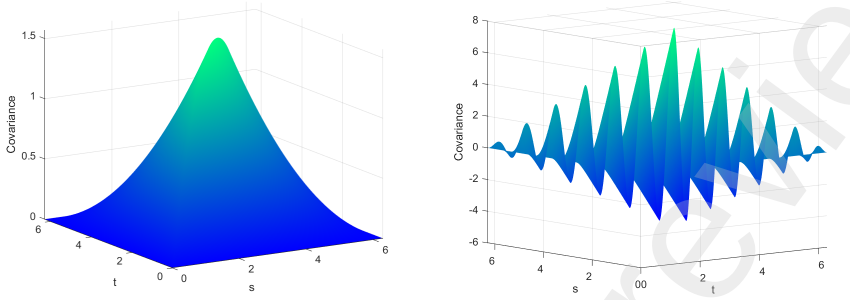
Figure 13: Comparison of non-Gaussian ACFs for different methods at truncation term $n = 5$. Top row: target, SAFD-ITAM computed, and KL-based computed ACFs for $\mathbf{C}_3$; bottom row: corresponding ACFs for $\mathbf{C}_4$.

Preprint not peer reviewed

This preprint research paper has not been peer reviewed. Electronic copy available at: https://ssrn.com/abstract=5360033

In this example, we also choose $p = 4$, $q = 2$. We set $\mu_B(t)$ to be zero for convenience. Solving (44) and (??) yields,

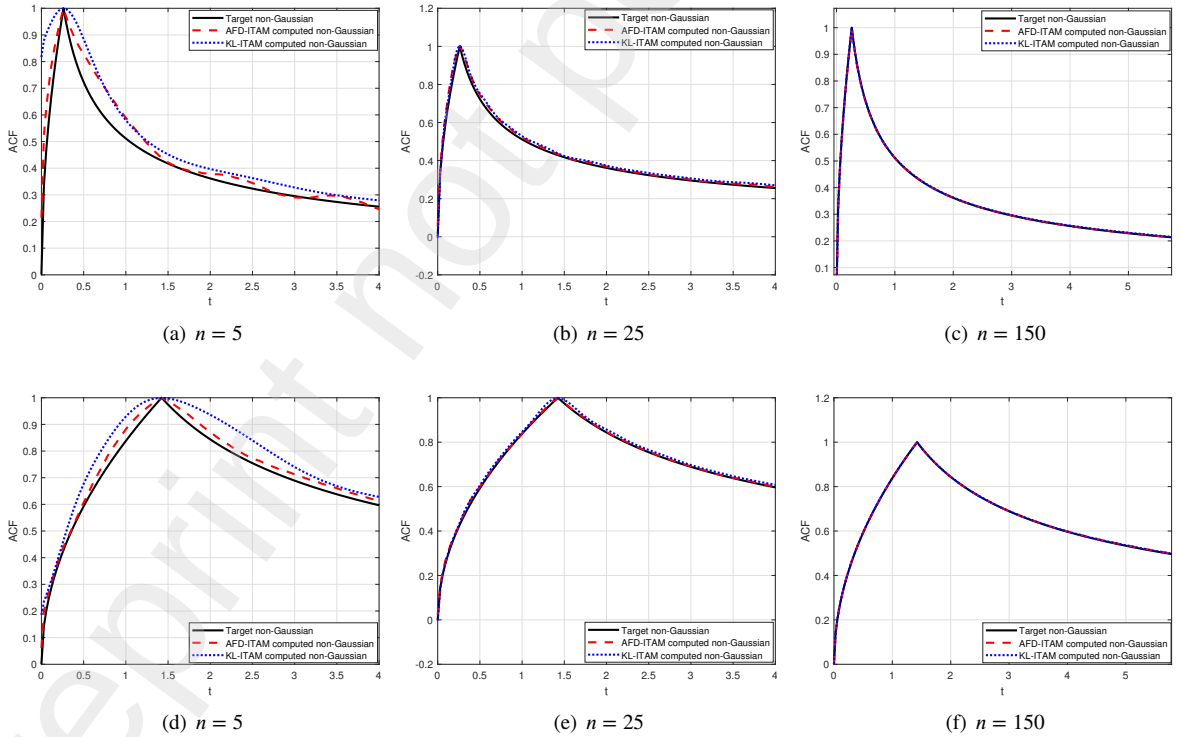
$$y_{min}(t) = -\sqrt{14(t - \frac{t^2}{2\pi})},\ y_{max}(t) = \sqrt{3.5(t - \frac{t^2}{2\pi})}. \tag{47}$$



(a) $\mathbf{C}_5$ (b) $\mathbf{C}_6$

Figure 14: Target non-stationary covariances $\mathbf{C}_5$ and $\mathbf{C}_6$.

Under the non-stationary condition, Figure 15 compares the target non-Gaussian ACF with those computed using the SAFD-ITAM and KL-ITAM methods, focusing on the 10th and 50th rows of the covariance matrix $\mathbf{C}_5$. In this non-stationary case, both methods perform well, and SAFD-ITAM continues to exhibit rapid convergence.



(a) $n = 5$ (b) $n = 25$ (c) $n = 150$

(d) $n = 5$ (e) $n = 25$ (f) $n = 150$

Figure 15: Comparison of target non-Gaussian, AFD-ITAM computed non-Gaussian, and KL-ITAM computed non-Gaussian ACFs. Top row: results for the $10th$ row of $\mathbf{C}_5$ with different truncation terms n; bottom row: corresponding results for the $50th$ row of $\mathbf{C}_5$.

Preprint not peer reviewed

This preprint research paper has not been peer reviewed. Electronic copy available at: https://ssrn.com/abstract=5360033

Figure 16 further illustrates that even with a small truncation term, SAFD-ITAM still achieves accurate reconstruction. Table 4, corresponding to the results for covariance matrix $\mathbf{C}_5$, quantifies this advantage: at $n = 5$, the error of SAFD is 58.7 % lower than that of KL (0.0368 vs. 0.0890).

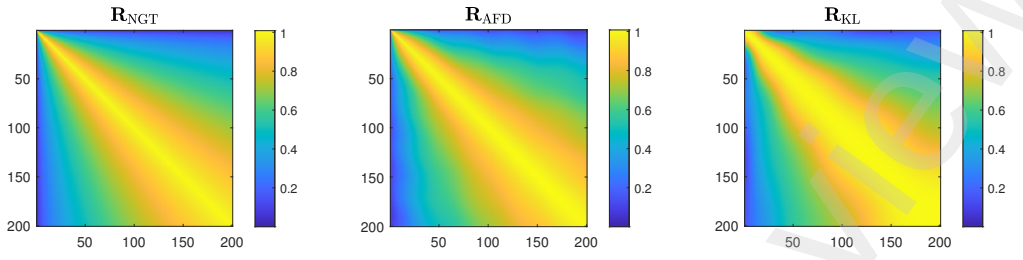


Figure 16: Comparison of non-Gaussian ACFs for different methods at truncation term $n = 5$. target, AFD-ITAM computed, and KL-based computed ACFs for $\mathbf{C}_5$.

Example 6.4. Non-stationary strongly non-Gaussian process *The marginal distribution function is also the shifted lognormal in (41). In the non-stationary non-Gaussian case, the target marginal distribution function varies with t. In this case, the shape of the distribution is given by σ, which is usually set to 1. Similarly, The parameters μ and σ can be represented by the mean and variance of this distribution (41).*

$$\mu_{SL}(t) = \delta(t) + e^{\mu(t)+\frac{\sigma^2}{2}}, \qquad \sigma^2_{SL}(t) = (e^{\sigma^2} - 1)e^{2\mu(t)+\sigma^2} \tag{48}$$

The target covariance function, as shown in Fig. 14 (b), combines a Brownian bridge structure with harmonic modulation,

$$\mathbf{C}_6(s,t) = \min(s,t) \cdot \cos[2\pi(s-t)], \quad \forall s,t \in [0,2\pi] \tag{49}$$

The variance function is

$$\sigma^2_{SL}(t) = \mathbf{C}_6(t,t) = t, \quad \forall t \in [0,2\pi].$$

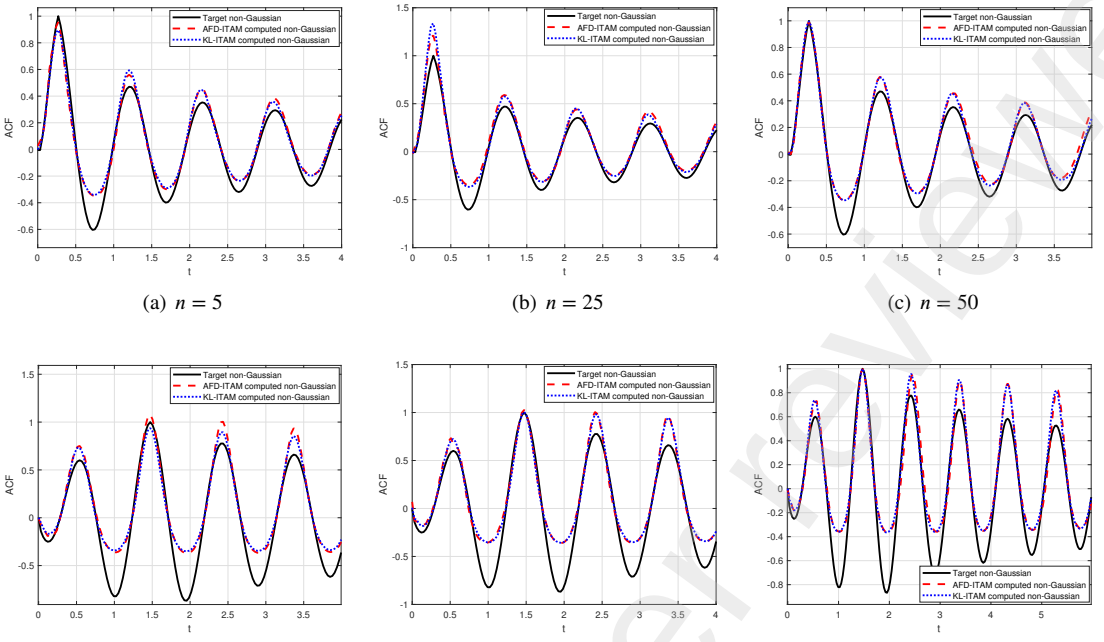
For simplicity, let $\mu_{SL} = 0$ and $\sigma = 1$. Solving (48) yield

$$\mu(t) = ln\sqrt{\frac{t}{e-1}} - \frac{1}{2}, \qquad \delta(t) = -\sqrt{\frac{t}{e-1}}. \tag{50}$$

Under the most complex framework of strongly non-Gaussian and non-stationary conditions, simulating a stochastic process that satisfies the prescribed properties is highly challenging. As shown in Figure 17, the simulation accuracy remains limited under such strongly non-Gaussian scenarios, which reflects the compatibility principle emphasized in Section 4. Within the ITAM algorithm framework, the entire procedure is designed around satisfying this compatibility condition. Once this condition is not met, the simulation results tend to deteriorate. Nevertheless, the general trend of the target process can still be clearly captured. Under this challenging setting, the rapid convergence property of SAFD-ITAM becomes less pronounced.

Preprint not peer reviewed

This preprint research paper has not been peer reviewed. Electronic copy available at: https://ssrn.com/abstract=5360033



(a) $n = 5$ (b) $n = 25$ (c) $n = 50$

(d) $n = 5$ (e) $n = 25$ (f) $n = 50$

Figure 17: Comparison of target non-Gaussian, SAFD-ITAM computed non-Gaussian, and KL-ITAM computed non-Gaussian ACFs. Top row: results for the $10th$ row of $\mathbf{C}_6$ with different truncation terms n; bottom row: corresponding results for the $50th$ row of $\mathbf{C}_6$.

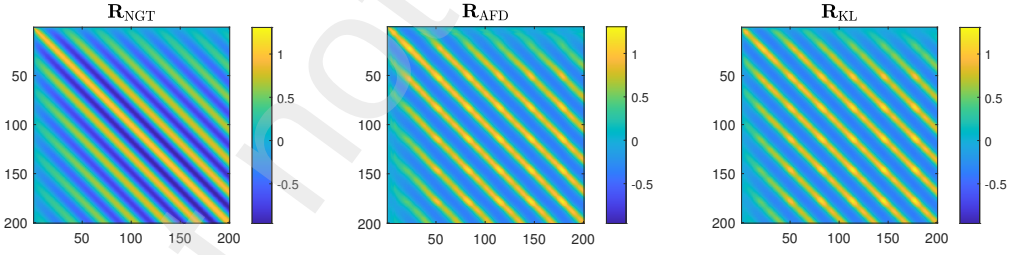


Figure 18: Comparison of non-Gaussian ACFs for different methods at truncation term $n = 5$. 5target, AFD-ITAM computed, and KL-based computed ACFs for $\mathbf{C}_6$.

Table 4
Comparison of global relative errors of covariance matrices across term.

Covariance Matrix	KL				SAFD			
	5	10	25	50	5	10	25	50
$\mathbf{C}_5$	0.0890	0.0510	0.0174	0.0025	0.0368	0.0322	0.0146	0.0023
$\mathbf{C}_6$	0.3938	0.3989	0.3920	0.3827	0.3902	0.3928	0.3913	0.3864

Preprint not peer reviewed

This preprint research paper has not been peer reviewed. Electronic copy available at: https://ssrn.com/abstract=5360033

7. Conclusion

This study proposes a novel theoretical framework of SAFD-ITAM for simulating non-Gaussian and non-stationary random processes with prescribed statistical properties. In this framework, the ITAM iterative algorithm avoids generating samples that match a given autocorrelation function and distribution; instead, it directly updates the target ACF through iteration. Meanwhile, the SAFD method achieves an analytical representation of the stochastic process by selecting an optimal adaptive dictionary. Compared to the traditional KL method, the proposed approach offers theoretical advantages by eliminating the need to solve the integral equations associated with covariance-induced integral operators, whose eigenvalues and eigenfunctions are typically obtained in numerical form. From a numerical perspective, the SAFD method also outperforms the KL method by achieving high accuracy with fewer decomposition terms, demonstrating faster convergence and improved computational efficiency. The results confirm the robustness and practicality of SAFD in complex stochastic modeling tasks, offering a promising alternative for applications requiring precise simulation of non-Gaussian and non-stationary behavior.

Declaration of Competing Interest

The authors declare that they have no known competing financial interests or personal relationships that could have appeared to influence the work reported in this paper.

Acknowledgement

The authors are grateful to Michael D. Shields (Johns Hopkins University) for his invaluable guidance on the algorithmic design of the ITAM method.

The research is supported by the Science and Technology Development Fund of Macau SAR [grant number FDCT0128/2022/A], the Zhejiang Provincial Natural Science Foundation of China [grant number LQ23A010014], and the Research Start-up Funding of Zhejiang University of Science and Technology, Third Quarter 2024 [grant number F701108P08].

Preprint not peer reviewed

This preprint research paper has not been peer reviewed. Electronic copy available at: https://ssrn.com/abstract=5360033

References

[1] R.C. Smith, Uncertainty Quantification: Theory, Implementation, and Applications[M]. SIAM, 2014.

[2] J. Li, J. Chen, Stochastic dynamics of structures[M], John Wiley & Sons, 2009.

[3] R.Y. Rubinstein, D.P. Kroese, Simulation and the Monte Carlo method[M], John Wiley & Sons, 2016.

[4] M. Grigoriu, Crossing of non-Gaussian translation processes[J], J. Eng. Mech. 110 (1984) 610–620, https://doi.org/10.1061/(ASCE)0733-9399(1984)110:4(610).

[5] F. Yamazaki, M. Shinozuka, Digital generation of non-Gaussian stochastic fields[J], J. Eng. Mech. 114 (1988) 1183–1197, https://doi.org/10.1061/(ASCE)0733-9399(1988)114:7(1183).

[6] R. Popescu, G. Deodatis, J.H. Prevost, Simulation of homogeneous nonGaussian stochastic vector fields[J], Probab. Eng. Mech. 13 (1998) 1–13, https://doi.org/10.1016/S0266-8920(97)00001-5.

[7] G. Deodatis, R. Micaletti, Simulation of highly skewed non-Gaussian stochastic processes[J], J. Eng. Mech. 127 (2001) 1284–1295, https://doi.org/10.1061/(ASCE)0733-9399(2001)127:12(1284).

[8] P. Bocchini, G. Deodatis, Critical review and latest developments of a class of simulation algorithms for strongly non-Gaussian random fields[J], Probab. Eng. Mech. 23 (2008) 393–407, https://doi.org/10.1016/j.probengmech.2007.09.001.

[9] N.D. Lagaros, G. Stefanou, M. Papadrakakis, An enhanced hybrid method for the simulation of highly skewed non-Gaussian stochastic fields[J], Comput. Methods Appl. Mech. Eng. 194 (2005) 4824–4844, https://doi.org/10.1016/j.cma.2004.12.009.

[10] M.D. Shields, G. Deodatis, P. Bocchini, A simple and efficient methodology to approximate a general non-Gaussian stationary stochastic process by a translation process[J], Probab. Eng. Mech. 26 (2011) 511-519, https://doi.org/10.1016/j.probengmech.2012.10.003.

[11] M.D. Shields, G. Deodatis, A simple and efficient methodology to approximate a general non-Gaussian stationary stochastic vector process by a translation process with applications in wind velocity simulation[J], Probab. Eng. Mech. 31 (2013) 19-29, https://doi.org/10.1016/j.probengmech.2012.10.003.

[12] Y. Wu, Y. Gao, A modified spectral representation method to simulate non-gaussian random vector process considering wave-passage effect[J], Eng. Struct. 201 (2019) 109587, https://doi.org/10.1016/j.engstruct.2019.109587.

[13] H. Zhou, G. Deodatis, M. Shields, B. Benowitz, Simulation of wind velocity time histories on long span structures modeled as non-Gaussian stochastic waves[J], Probab. Eng. Mech. 59 (2020) 103016, https://doi.org/10.1016/j.probengmech.2020.103016.

[14] B. Li, L. Peng, Y. Jiang, et al., Simulation of stationary non-Gaussian stochastic vector processes using an eigenvalue-based iterative translation approximation method[J], Mech. Syst. Signal Process. 175 (2022) 109128, https://doi.org/10.1016/j.ymssp.2022.109128.

[15] Y. Jiang, Y. Hui, Y. Wang, et al., A novel eigenvalue-based iterative simulation method for multi-dimensional homogeneous non-Gaussian stochastic vector fields[J], Struct. Saf. 100 (2023) 102290, https://doi.org/10.1016/j.strusafe.2022.102290.

[16] W. Hu, Q. Yang, L. Peng, et al., Non-stationary modeling and simulation of strong winds[J], Heliyon 10 (2024) e35195, https://doi.org/10.1016/j.heliyon.2024.e35195.

[17] K. Phoon, S. Huang, S. Quek, Simulation of second-order processes using Karhunen-Loève expansion[J], Comput. Struct. 80 (2002) 1049-1060, https://doi.org/10.1016/S0045-7949(02)00064-0.

[18] K. Phoon, H. Huang, S. Quek, Simulation of strongly non-Gaussian processes using Karhunen-Loève expansion[J], Probab. Eng. Mech. 20 (2005) 188-198, https://doi.org/10.1016/j.probengmech.2005.05.003.

[19] Z. Zheng, M. Beer, An iterative multi-fidelity scheme for simulating multi-dimensional non-Gaussian random fields[J], Mech. Syst. Signal Process. 200 (2023) 110643, https://doi.org/10.1016/j.ymssp.2023.110643.

[20] Y. Li, J. Xu, Neural network-aided simulation of non-Gaussian stochastic processes[J], Reliab. Eng. Syst. Saf. 242 (2024) 109786, https://doi.org/10.1016/j.ress.2023.109786.

[21] Z. Zhao, Z.H. Lu, Y.G. Zhao, Simulating multivariate stationary non-Gaussian process based on wave number frequency spectrum and unified Hermite polynomial model[J], Probab. Eng. Mech. 69 (2022) 103272, https://doi.org/10.1016/j.probengmech.2022.103272.

[22] Z. Zhao, Z.H. Lu, X.Y. Zhang, Y.G. Zhao, Simulating multivariate multidimensional homogenous non-Gaussian field based on unified Hermite polynomial model[J], J. Eng. Mech. 149 (2023) 06023001, https://doi.org/10.1061/JENMDT.EMENG-6996.

[23] Z. Zhao, Z.H. Lu, Y.G. Zhao, Simulating non-stationary and non-Gaussian cross-correlated fields using multivariate Karhunen-Loève expansion and L-moments-based Hermite polynomial model[J], Mech. Syst. Signal Process. 216 (2024) 111480, https://doi.org/10.1016/j.ymssp.2024.111480.

[24] H. Dai, Z. Zheng, H. Ma, An explicit method for simulating non-gaussian and non-stationary stochastic processes by Karhunen-Loève and polynomial chaos expansion[J], Mech. Syst. Signal Process. 115 (2019) 1-13, https://doi.org/10.1016/j.ymssp.2018.05.026.

[25] W. Qu, Y. Zhang, T. Qian, Sparse representation of random field via probability chaos[J], Math. Methods Appl. Sci. (2025), https://doi.org/10.1002/mma.11167.

[26] Y. Zhang, W. Qu, H. Zhang, T. Qian, Simulation of non-stationary and non-Gaussian stochastic processes by the AFD-Type Sparse Representations[J], Mech. Syst. Signal Process. 204 (2023) 110762, https://doi.org/10.1016/j.ymssp.2023.110762.

[27] Z. Zheng, H. Dai, Y. Wang, W. Wang, A sample-based iterative scheme for simulating non-stationary non-Gaussian stochastic processes[J], Mech. Syst. Signal Process. 151 (2021) 107420, https://doi.org/10.1016/j.ymssp.2020.107420.

[28] H. Kim, M.D. Shields, Modeling strongly non-Gaussian non-stationary stochastic processes using the iterative translation approximation method and Karhunen-Loève expansion[J], Comput. Struct. 161 (2015) 31-42, https://doi.org/10.1016/j.compstruc.2015.08.010.

[29] T. Qian, Sparse representation of random signals[J], Math. Meth. Appl. Sci. 45 (2022) 4210-4230, https://doi.org/10.1002/mma.8033.

[30] G.J. Lord, C.E. Powell, T. Shardlow, An Introduction to Computational Stochastic PDEs[M], Cambridge University Press, 2014.

[31] T.Y. Hou, W. Luo, B. Rozovskii, H.M. Zhou, Wiener chaos expansions and numerical solutions of randomly forced equations of fluid mechanics[J], J. Comput. Phys. 216 (2006) 687-706, https://doi.org/10.1016/j.jcp.2006.01.008.

[32] C. Schwab, R.A. Todor, Sparse finite elements for elliptic problems with stochastic loading[J], Numer. Math. 95 (2003) 707-734, https://doi.org/10.1007/s00211-003-0455-z.

Preprint not peer reviewed

This preprint research paper has not been peer reviewed. Electronic copy available at: https://ssrn.com/abstract=5360033

[33] T. Qian, Y.B. Wang, Adaptive Fourier series a variation of greedy algorithm[J], Adv. Comput. Math. 34 (2011) 279-293, https://doi.org/10.1007/s10444-010-9153-4.
[34] T. Qian, Y. Zhang, W.Q. Liu, W. Qu, Adaptive Fourier decomposition-type sparse representations versus the Karhunen-Loève expansion for decomposing stochastic processes[J], Math. Method. Appl. Sci. (2023), https://doi.org/10.1002/mma.9301.
[35] H.L. Van Trees, Detection, estimation, and modulation theory, part I: Detection, estimation, and linear modulation theory[M], Wiley, 2004.
[36] M. Grigoriu, E. Harper, Applied non-Gaussian processes: examples, theory, simulation, linear random vibration, and MATLAB solutions[M], Prentice Hall, 1995.
[37] F. Ferrante, S. Arwade, L. Graham-Brady, A translation model for non-stationary, non-Gaussian random processes[J], Probab. Eng. Mech. 20 (2005) 215-228, https://doi.org/10.1016/j.probengmech.2005.05.003.
[38] N.J. Higham, Computing the nearest correlation matrix a problem from finance[J], IMA J. Numer. Anal. 22 (2002) 329-343, https://doi.org/10.1093/imanum/22.3.329.

Preprint not peer reviewed

This preprint research paper has not been peer reviewed. Electronic copy available at: https://ssrn.com/abstract=5360033